

A PDE-based log-agnostic illumination correction algorithm

Uche A. Nnolim¹

Department of Electronic Engineering, University of Nigeria, Nsukka, Enugu, Nigeria

Abstract

This report presents the results of a partial differential equation (PDE)-based image enhancement algorithm, for dynamic range compression and illumination correction in the absence of the logarithmic function. The proposed algorithm combines forward and reverse flows in a PDE-based formulation. The experimental results are compared with algorithms from the literature and indicate comparable performance in most cases..

Keywords: Image edge contrast enhancement; illumination-reflectance model; filter kernel-based enhancement; log-agnostic dynamic range compression; power law-based illumination correction; partial differential equations

1. Introduction

Image enhancement is a vital preprocessing stage in image processing as it enables improved depiction of features for better analysis and extraction [1]. The feature to be enhanced include contrast, edge or colour attributes of images and several algorithms for achieving this are found in the literature and range from simple to complex algorithms [1] [2]. In the case of this work, we focus on tone mapping operation (TMO)-based algorithms, which are used to render high dynamic range (HDR) images on low dynamic range (LDR) display and print devices [1].

Examples of these TMOs include the Homomorphic [3] and Retinex [4] filters. Other algorithms include the fusion-based approaches [5], entropy-based wavelet coefficient scaling (ESWD) [6], spatially guided filtering [7], Gamma Correction (GGC) [8], Generalized Unsharp Masking (GUM) [9] algorithms [8] [10] and naturalness restoration [11]. Others include the relatively recent partial differential equations (PDE)-based enhancement by Sapiro and Caselles [12], Provenzi, et al [13], variational Retinex framework by Kimmel, et al [14], and others by [15] [16] [17] [18] [19], PDE-based Homomorphic filter (PDE-HF) [20], Dynamic Stochastic Resonance (DSR) [21], Bayesian [22] probabilistic schemes [23] and recent works such as entropy-guided Retinex-boosted AD [24], global sparse gradient guided variational Retinex (GSG-VR) [25] and variational low-light image enhancement using optimal transmission map [26].

PDE-based approaches are more versatile and flexible in addition to being able to yield intermediate and gradual results [27]. However, these algorithms do not have a means of obtaining the optimum result or an image measure-based guided approach to determine stopping time of the various PDE-based algorithms, which must be tuned to obtain good results for different images. Additionally, sub-par results are observed for several of the approaches, where there is minimal illumination normalization or considerable colour fading. Conversely, others over-enhance the images, leading to sharp divisions between light and dark regions in terms of over-exposure and under-exposure, respectively. Furthermore, most of these algorithms do not have easily implementable structure that can be developed in digital hardware

2. Relevant prior work

Several algorithms have attempted to solve the illumination estimation and reflectance extraction problem in a fast and compact but near accurate way and popular examples of such earlier methods are the HF and Retinex methods. The initial approaches employed the logarithmic image processing (LIP) model [1], symmetric LIP (SLIP) [8], [28] and parametric log models [29]. Additionally, variational approaches [13] [14] [15] [16] [17] [18] [19] combined with Bayesian probabilistic framework [23] have also been proposed in addition to recent works [24], [25] and [26]. Each of these methods have the strengths and weaknesses and some may exhibit high computational complexity. Additionally, these methods are not easily amenable to hardware implementation due to their structure.

The proposed tonal mapping algorithm is adaptive and guided by image metrics to ensure optimum results with the ability to process both dark and faded images while using small spatial filter kernel-based operators and avoiding logarithmic operations in a PDE-based formulation. Additionally, it attempts to solve the problem of difficulty of hardware realization by utilizing spatial filter structures to approximate these PDE processes. Furthermore, its avoidance of logarithm removes the need to implement logarithm functions for embedded mobile devices, which do not support such functions. Moreover, the algorithm has a dual-use function as it can be used to process either dark or faded, low-contrast images by adjustment of the contributions of these processes. The proposed approach also expands the discussion to generalize the algorithm to any domain that possesses contra-opposing processes for high- or low-frequency components.

3. Proposed algorithm

The proposed scheme can be realized in the frequency or spatial domain [30] as shown in (1);

$$I_e(x, y) = \varphi\{I_{HPF}(x, y)\} + \gamma\{I_{LPF}(x, y)\} \quad (1)$$

Where $\varphi\{\}$ and $\gamma\{\}$ are amplification and attenuation functions for the high-pass, $I_{HPF}(x, y)$ and low-pass, $I_{LPF}(x, y)$ images respectively [30] and $I_e(x, y)$ is the enhanced image. In previous work, we used the following expression to obtain the enhanced output image;

$$I_e(x, y) = I_{HPF}(x, y) + \sqrt{I_{LPF}(x, y)} \quad (2)$$

The PDE-based formulation can then be realized after derivation as;

$$\frac{\partial I(x, y, t)}{\partial t} = \lambda(-\nabla^2 I(x, y, t) + [D - 1]^{1-k}\{I(x, y, t) + \nabla^2 I(x, y, t)\}^k - I(x, y, t)) + \frac{\beta(I(x, y, t) - \mu)}{\sigma} \quad (3)$$

From which we minimize the energy functional;

$$E(I) = \int_{\Omega} \lambda(-\nabla^2 I(x, y, t) + [D - 1]^{1-k}\{I(x, y, t) + \nabla^2 I(x, y, t)\}^k - I(x, y, t)) + \frac{\beta(I(x, y, t) - \mu)}{\sigma} dx dy \quad (4)$$

It should be noted that the system can be generalized to any domain but for run-time purposes, we choose to utilize spatial filter or frequency domain filters. For hardware implementation, it would make sense to utilize spatial filter kernel structures, since these architectures can be easily established using hardware description language (HDL) in digital hardware such as FPGAs [30].

Experiments performed to analyze the system are shown in Fig. 1 concerning the relationship between the regularization parameter, λ and the number of required iterations. In general, the lower the value of the parameter, the more iterations needed to attain maximum entropy, which is our optimization goal in this case. Thus, in summary, the parameter influences the execution time of the algorithm.

Additionally, some images may require much more enhancement and, thus the algorithm may be slower in attaining the optimization goal (will run for more cycles), especially if little variations are made over time rather than more drastic ones. However, this is a strength in that the approach is able to improve under-exposed regions without over-enhancing the bright regions and losing details in the process, unlike closed-form algorithms.

4. Experiments

In this section, we tested the proposed approach against several algorithms from the literature such as global histogram equalization (GHE), adaptive HE (AHE), contrast limited AHE (CLAHE) [31], histogram specification (HS) [32], gain offset correction (GOC1, GOC2 and GOC3) [33], piecewise linear transform (PWL) [34], linear contrast stretching (CS/LCS) [35], splitting signal alpha rooting (SSAR) [36], tonal correction (TC) [37], spatial and frequency domain HF (SHF and FDHF) [1] [38], single and multiscale Retinex with colour restoration (SSR, MSR and MSRCR) [39] [4] and GUM [9] and PDE-based formulations from earlier work [40].

We tested over 195 dark images from various sources including benchmark images used by several authors from the literature and others from the internet. Additionally, run-time comparisons were performed to assess time-complexity

of the available algorithms. We performed numerical comparisons using image quality metrics such as colour enhancement factor (CEF) [41], relative mean brightness (RM), relative standard deviation (RSD) [42], relative entropy (RE), relative average gradient (RAG) [43], hue deviation index (HDI) [43] and perceptual quality metric (PQM) [21]. The relative values represent a ratio of output over input images, thus values greater than unity signify improvement, while those less than unity imply degradation. The HDI ideally should be less than one for good hue preservation while PQM should be as close to 10 as possible, where 10 is the ideal value.

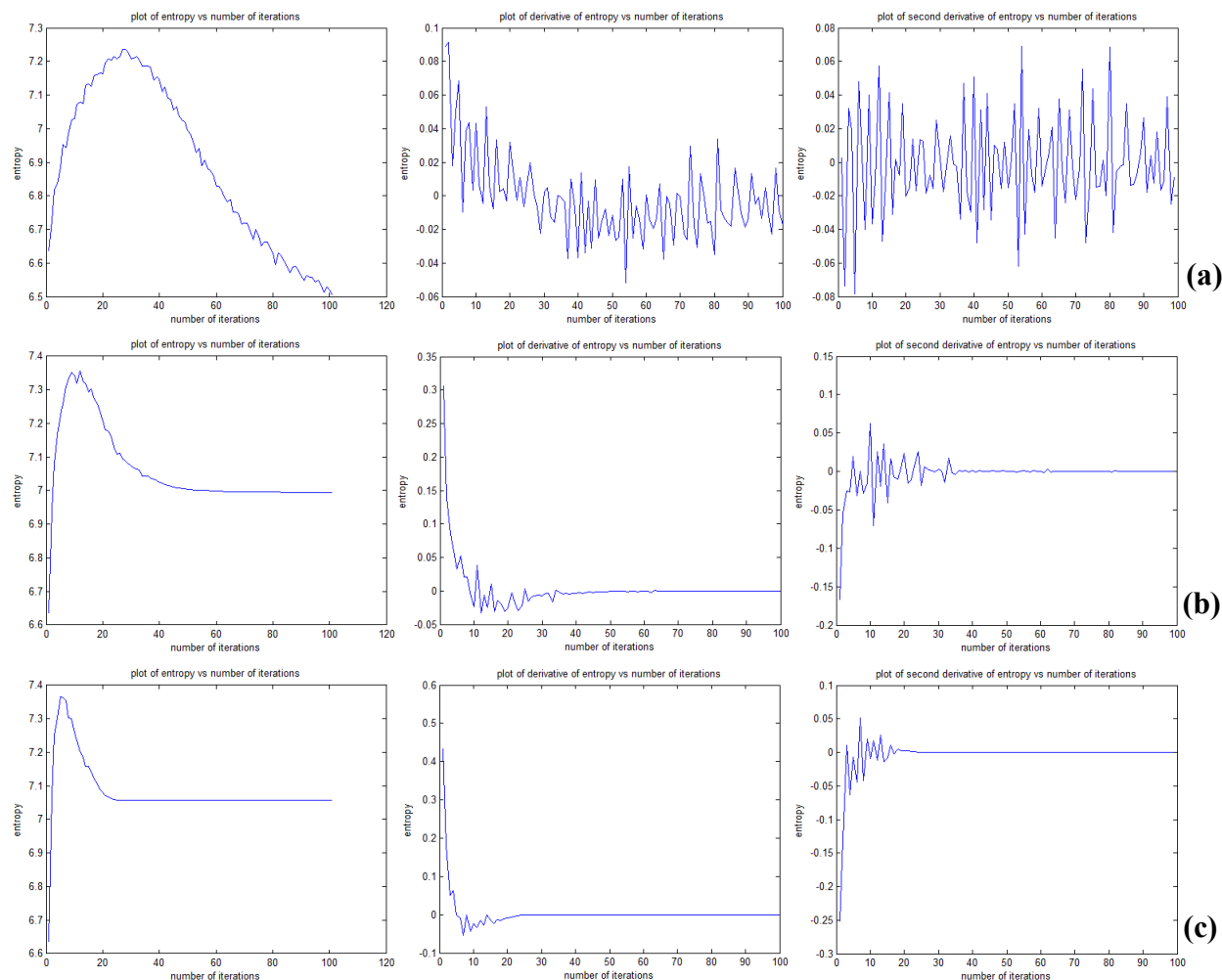


Fig. 2 Entropy, first derivative and second derivative of entropy with respect to number of iterations for intensity channel of *Iris* image processed with PA for (a) $\lambda = 0.1$, (b) $\lambda = 0.5$ and (c) $\lambda = 1$ for 100 iterations

However, we keep in mind that numerical results based on no-reference metrics especially in the domain of illumination correction-based image enhancement is difficult to reconcile objective results with visual outcomes. This is because image colour and contrast aesthetics are not clearly quantified by numerical values, which measure structural changes but may not be precise in relating to perceptual results. We therefore focus on consistent mid-range values to represent a balanced result than obtaining extremely high or low values with usually poor visual result as will be seen in the subsequent figures.

4.1 Visual evaluation

In Fig.2, we provide the key to Fig. 3 where we present the visual and corresponding numerical results for the *Swan*, *Notre Dame*, *Big Ben* and *Horse* images. Based on results, the PDE-based formulations of the closed-form algorithms improve result for algorithms such as CLAHE. However, over-enhancement is observed in the swan's feathers. Most of the other algorithms darken the under-exposed regions and brighten the over-exposed regions as expected. The HF

brightens the image but yields flattened and faded colours, while multi-scale Retinex algorithms give high contrast but with darkened regions and grey colouration in the white regions of the image. The worst performing algorithms are the GUM and SSR, statistical-based algorithms such as GHE, AHE, HS, which over-expose and over-enhance the entire image and distort the colours, while SSAR darkens the image. Conversely, PA brightens the dark regions of the image, while avoiding the over-exposure of bright regions, yielding a balanced result.

For the *Notre Dame* image, results are similar except that PA results in a faded sky similar to the HF, though it is less than the HF. Most of the other algorithms do not show any visible improvement or rather much worse results. Only the PDE-based CLAHE variants yield richer colours though with over-enhanced sky regions with halos and slight under-exposed dark regions while others have distorted colours. The GUM, SSR and global histogram stretching algorithms yield the worst results.

For the *Big Ben* image, the PA and HF yield similar results with faded colours in the sky regions, while the Retinex, CLAHE and others darken the image without resolution of dark regions. As usual the other statistics-based algorithms exhibit a pseudo thresholding effect by darkening under-exposed regions while brightening light areas, losing details. SSR and GUM yield over-bright images while SSAR darkens the image.

For the *Horse* image, once more, the PA and HF yield similar and best results, while the Retinex, CLAHE and others darken the image and statistics-based algorithms cannot resolve the under-exposed regions losing details in bright regions. The SSR and GUM yield over-bright images (though to a lesser extent compared with their previous performance) while SSAR once more darkens the image.

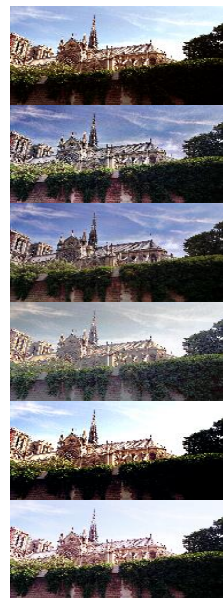
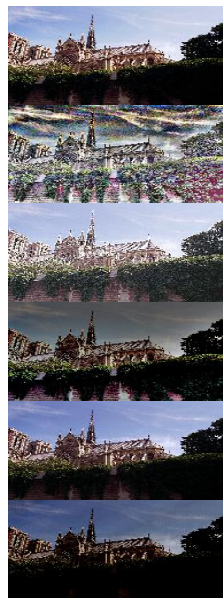
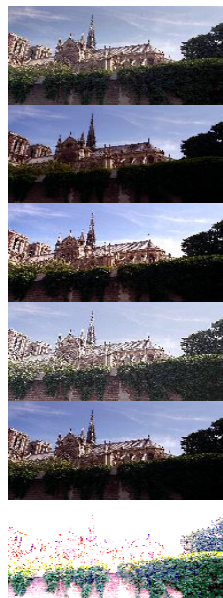
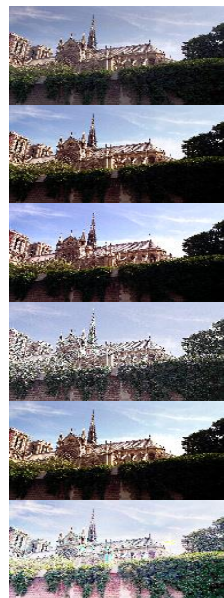
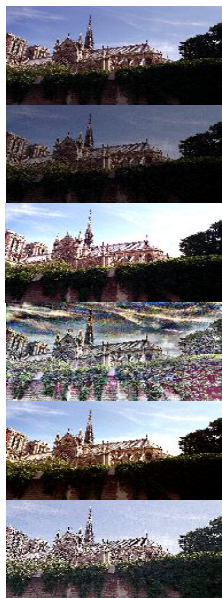
In Fig. 4, we compare visual results of PA with discrete cosine transform (DCT)-based enhancement (CES) [44], direct image contrast enhancement (DICE) [45], variational perceptually-inspired colour enhancement (VPCE) [13], image Gaussian illumination enhancement (IEGP) [46], MSR [4] and ESWD [6] from the literature [6]. Results indicate that PA surpasses several of the algorithms while being comparable to the best versions. In Fig. 5, we present additional results for PA for a wide array of images with varying levels of uneven illumination and we can see that it has problems with local contrast performance, which is expected in some cases. In Fig. 6, we also compare the PA against SLIP- based generalized gamma correction (SLIP-GGC) [8], LCS, CLAHE, local color correction (LCC) [47] [48], adaptive gamma correction (AGC) [49] and parametric log-ratio model (PLR) [50] using the figures from [8] amended with result from PA. Numerical results in Table 1 to 4 (Table 4 is from [8] amended with PA) indicate that PA yields balanced results, which are not at the extremes of too low or too high and this is in line with its visual results being subtle in enhancement unlike the other algorithms with extreme visual outcomes indicating distortions. This does not mean that PA cannot be modified to yield much higher numerical values but this would also defeat the purpose of gradual enhancement. Additionally, it should be stated that no algorithm can yield the best results for all possible images due to the uniqueness of images and their structural and perceptual features in addition to human subjective evaluation.

Original Image	PDE_HS	PDE_GOC2	PDE_GOC3	PDE_PWL	PDE_GHE
PDE_CE	PDE_CS	PDE_MINMAX	PDE_AHE	PDE_CLAHE	CP_PDE_CLAHE
ADE1	ADE3	MCECR	MCECR_HF	MCECR_CLAHE	CLAHE
AHE	SHF	FDHF	MSR	GHE	HS
PWL	CS	GOC1	GOC2	GOC3	RGB-IV-PA
HSI-PA	GUM	SSR	SSAR	TC	MSRCR

Fig. 2 Key to figure 3



(a)



(b)

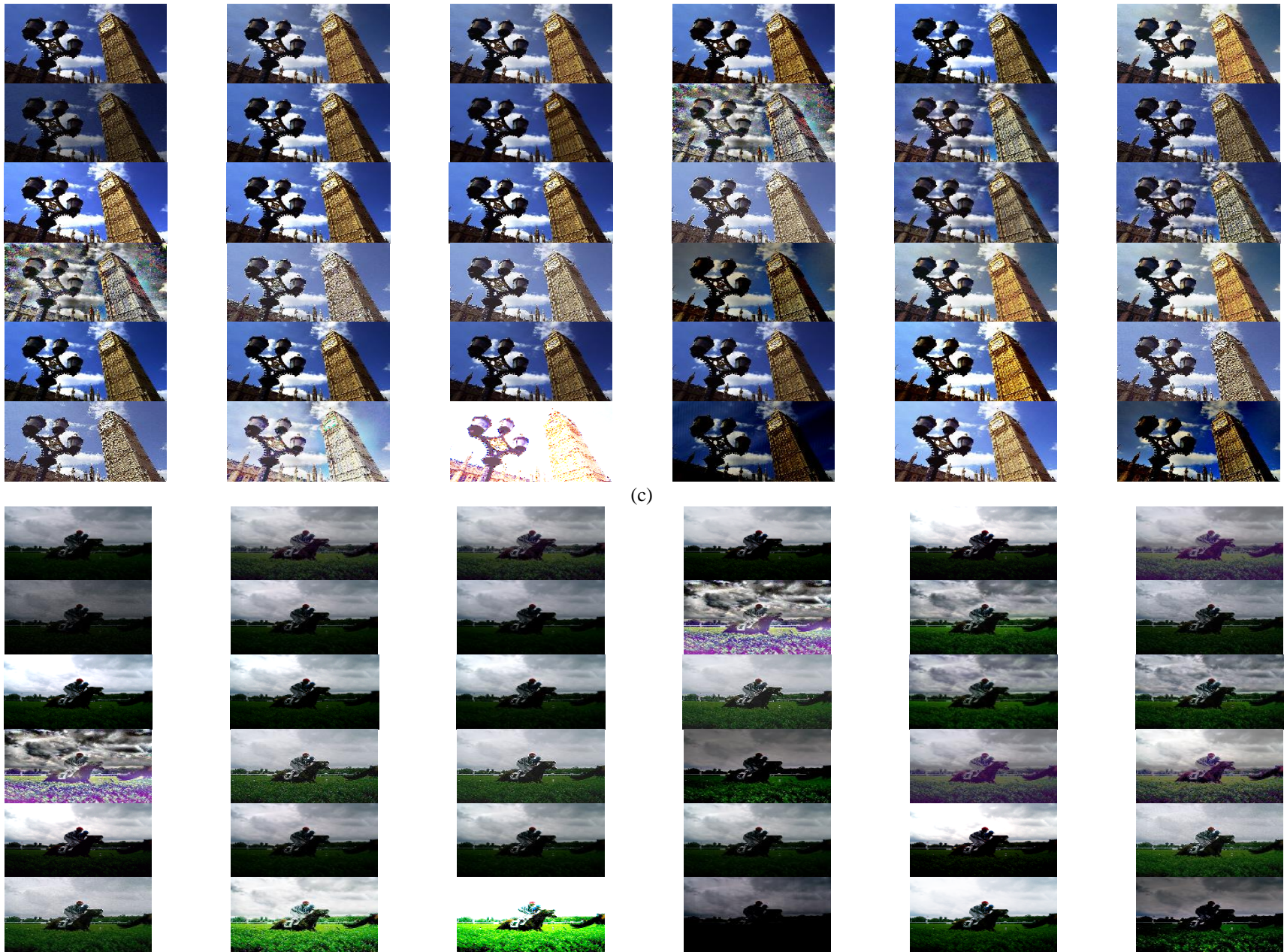


Fig. 3 (a) Swan, (b) Notre Dame (c) Big Ben (d) Horse images processed with various algorithms

4.2 Objective evaluation

In Table 1, we present the initial obtained metrics for the sample images under test and their corresponding numerical results obtained from processing with various algorithms compared with the proposed approach (PA) in Table 2.

Table 1 Initial numerical values for the sample test images

Swan	Notre Dame	Big Ben	Horse
Colourfulness = 15.63302 Sigma = 62.46685 Mu = 52.18342 Entropy = 6.564669 AG = 5.813808 EMEC = 13.43151	Colourfulness = 35.278 Sigma = 79.34511 Mu = 87.01462 Entropy = 7.349838 AG = 8.174997	Colourfulness = 49.83381 Sigma = 64.83871 Mu = 81.48279 Entropy = 7.624601 AG = 7.025566 EMEC = 94.12284	Colourfulness = 11.99735 Sigma = 73.42452 Mu = 76.9868 Entropy = 6.457309 AG = 1.717612 EMEC = 94.12284

Table 2 Quantitative comparison of PA with popular algorithms for (a) *Swan* (b) *Notre Dame* (c) *Big Ben* and (d) *Horse* images

(a)

Algos\Measures	CMB	mu_o	sigma_o	ent_o	AG_o
PDE_HS	21.41041	85.11685	63.63443	7.612304	11.00838
PDE_GOC2	21.41041	85.11685	63.63443	7.612304	11.00838
PDE_GOC3	19.15079	75.26498	66.61575	6.792743	7.594429
PDE_PWL	19.68157	52.91116	74.50446	6.479009	7.082669
PDE_GHE	36.67305	128.5168	71.73287	7.068746	17.83355
PDE_CE	10.38371	31.89485	38.62476	6.173844	5.474874
PDE_CS	18.87627	53.33921	72.25838	6.531533	6.860005
PDE_MINMAX	14.04993	47.5424	61.91476	6.292792	3.242516
PDE_AHE	38.53974	123.6227	68.53655	7.969447	25.05661
PDE_CLAHE	26.11403	79.63	60.62871	7.489354	12.39316
CP_PDE_CLAHE	17.46621	65.01815	60.80349	7.069814	9.788868
ADE1	24.18329	75.18794	78.95176	6.169831	8.555037
ADE3	21.45112	62.59427	77.6474	6.285439	7.763636
MCECR	20.35833	60.66397	75.73802	6.463007	7.394342
MCECR_HF	20.67793	108.9197	60.66652	7.287016	13.55593
MCECR_CLAHE	21.19553	70.48403	59.01643	7.258112	7.004399
CLAHE	25.45356	80.00689	59.58507	7.497631	13.24651
AHE	38.53974	123.6227	68.53655	7.969447	25.05661
SHF	21.32438	106.7087	62.67002	7.42941	17.00257
FDHF	20.42786	107.5572	59.97325	7.323166	13.52661
MSR	25.77048	58.80421	65.43866	6.308283	12.38959
GHE	36.67305	128.5168	71.73287	7.068746	17.83355
HS	38.0407	127.4585	73.90013	8	17.79277
PWL	19.68157	52.91116	74.50446	6.479009	7.082669
CS	19.97168	53.39783	75.27249	6.373934	7.168449
GOC1	15.9899	52.74422	63.1567	6.568948	5.886273
GOC2	15.9899	52.74422	63.1567	6.568948	5.886273
GOC3	25.6736	104.934	74.13145	6.28182	9.922227
PA_2B	16.04195	76.82663	58.62702	7.037469	10.5224
PA_1A	16.04195	76.82663	58.62702	7.037469	10.5224
GUM	30.75108	163.8607	55.27601	7.67875	16.64929
SSR	23.46357	234.8064	31.15657	3.204113	8.721495
SSAR	14.30069	27.92414	54.50812	3.931229	3.989597
TC	25.40632	97.13901	73.3573	6.218762	10.63997
MSRCR	36.28314	51.58774	73.59523	5.054237	11.4534

(b)

Algos\Measures	CMB	mu_o	sigma_o	ent_o	AG_o
PDE_HS	24.46659	104.7324	75.92855	7.813199	8.967406
PDE_GOC2	24.46659	104.7324	75.92855	7.813199	8.967406
PDE_GOC3	30.30046	101.6759	92.6909	7.107077	8.974489
PDE_PWL	33.52995	110.5344	101.3294	6.720015	9.666191
PDE_GHE	22.48975	129.0636	72.4258	7.528004	10.11233
PDE_CE	21.61371	53.38676	48.52932	6.636064	6.54662
PDE_CS	31.11723	103.5883	92.74777	7.307866	9.295889
PDE_MINMAX	35.31877	78.78375	77.61752	7.101104	3.724257
PDE_AHE	37.20773	123.6673	66.02383	7.950476	25.20219
PDE_CLAHE	34.20047	101.0546	72.42216	7.506185	12.99812
CP_PDE_CLAHE	34.16708	95.65669	77.36181	7.580594	11.22214
ADE1	30.79586	124.7286	106.5112	6.023334	10.41408
ADE3	37.26559	111.7692	99.21694	6.929896	9.709866
MCECR	37.5011	107.3925	96.07697	7.158356	9.473395
MCECR_HF	24.29221	135.8742	80.3449	7.657615	15.08135
MCECR_CLAHE	34.54543	95.36644	72.29926	7.717245	7.682218
CLAHE	32.83629	100.3756	71.74582	7.500375	13.56241
AHE	37.20773	123.6673	66.02383	7.950476	25.20219
SHF	25.48615	135.4368	82.8546	7.669938	19.61284
FDHF	24.25264	134.2512	79.57425	7.665886	15.13771
MSR	21.05406	59.37361	53.67344	5.571938	9.142272
GHE	22.48975	129.0636	72.4258	7.528004	10.11233
HS	22.7633	127.5	73.9003	8	10.09779
PWL	33.52995	110.5344	101.3294	6.720015	9.666191
CS	31.06287	108.7171	97.06632	7.156449	9.631731
GOC1	35.278	87.01462	79.34511	7.349838	8.174997
GOC2	35.278	87.01462	79.34511	7.349838	8.174997
GOC3	33.24443	120.4932	111.2518	5.216588	10.09699
PA	24.74545	124.2023	87.26492	7.494009	19.13665
GUM	33.53043	170.611	75.53924	7.394675	16.28864
SSR	46.49454	205.2761	78.58745	2.872876	13.64984
SSAR	29.29079	47.71003	56.1948	4.605421	5.308647
TC	27.52768	136.189	101.5982	6.528876	10.983
MSRCR	28.05914	52.1765	54.4629	5.283449	9.088958

(c)

Algos\Measures	CMB	mu_o	sigma_o	ent_o	AG_o
PDE_HS	41.33353	101.5961	67.18735	7.86657	7.893266
PDE_GOC2	41.33353	101.5961	67.18735	7.86657	7.893266
PDE_GOC3	55.87024	97.32826	76.01511	7.611512	8.237562
PDE_PWL	68.97646	95.15653	80.27077	7.25373	8.331307
PDE_GHE	45.59658	128.6106	73.16487	7.691652	9.175682
PDE_CE	30.55856	49.85355	39.86509	6.9508	5.719523
PDE_CS	55.38993	91.98981	73.59688	7.588292	7.9884
PDE_MINMAX	49.91738	75.97098	63.29997	7.530192	4.066776
PDE_AHE	41.20839	119.6787	66.66957	7.943151	18.60902
PDE_CLAHE	42.56839	99.47617	63.47974	7.795666	11.23637
CP_PDE_CLAHE	48.78202	89.99641	63.53858	7.714931	9.738881
ADE1	76.63968	121.266	86.91034	6.969643	9.351299
ADE3	64.82332	108.5387	81.34196	7.412809	8.864436
MCECR	61.65622	103.6403	78.84124	7.49019	8.539138
MCECR_HF	41.17095	139.1162	64.77145	7.726807	12.3757
MCECR_CLAHE	42.17686	94.71956	60.08943	7.758456	7.365915
CLAHE	43.67208	96.68514	61.74161	7.763405	11.91487
AHE	41.20839	119.6787	66.66957	7.943151	18.60902
SHF	41.75646	137.7719	66.60855	7.733826	15.42066
FDHF	40.7758	137.0895	64.11581	7.737171	12.40638
MSR	36.25065	69.71917	55.87098	6.510649	7.541222
GHE	45.59658	128.6106	73.16487	7.691652	9.175682
HS	45.91335	127.4779	73.89831	8	9.076885
PWL	68.97646	95.15653	80.27077	7.25373	8.331307
CS	57.18495	95.04755	76.28879	7.402076	8.277622
GOC1	49.83381	81.48279	64.83871	7.624601	7.025566
GOC2	49.83381	81.48279	64.83871	7.624601	7.025566
GOC3	71.02618	117.7116	92.82944	6.245817	9.881299
PA_2B	42.26727	129.6407	70.63227	7.682708	16.59522
PA_1A	42.26727	129.6407	70.63227	7.682708	16.59522
GUM	42.19889	179.4507	59.37748	7.574447	11.675
SSR	51.7097	233.9467	51.76643	1.909429	7.851679
SSAR	39.59303	37.65087	48.77306	5.352086	5.184091
TC	58.78623	144.173	80.80218	7.093402	9.588547
MSRCR	55.10485	61.47176	63.31255	6.144844	7.80667

(d)

Algos\Measures	CMB	mu_o	sigma_o	ent_o	AG_o
PDE_HS	14.39133	99.08217	72.66473	7.611935	3.746073
PDE_GOC2	14.39133	99.08217	72.66473	7.611935	3.746073
PDE_GOC3	11.29153	95.65477	90.88007	6.340069	1.970514
PDE_PWL	11.65842	112.4371	104.6785	6.198049	2.326264
PDE_GHE	22.01073	116.1428	58.05779	6.760153	4.086882
PDE_CE	7.884665	47.40972	44.73713	5.911963	2.386313
PDE_CS	12.10946	85.81693	81.738	6.542314	1.916801
PDE_MINMAX	11.89701	76.00692	73.561	6.164958	1.204559
PDE_AHE	47.13342	133.6771	54.90483	7.76614	11.51669
PDE_CLAHE	26.78164	84.53481	70.30413	6.876912	4.020784
CP_PDE_CLAHE	15.21239	83.25001	73.40733	6.642108	3.147387
ADE1	19.12352	117.4214	109.3717	5.672184	2.412008
ADE3	14.67429	102.3854	97.06013	6.351584	2.225564
MCECR	13.91154	97.65126	92.94595	6.583243	2.130172
MCECR_HF	23.39278	122.1327	79.73324	7.111243	4.970293
MCECR_CLAHE	25.37082	81.77472	71.20501	6.978516	2.555353
CLAHE	23.73371	83.95083	68.66829	6.764479	4.265469
AHE	47.13342	133.6771	54.90483	7.76614	11.51669
SHF	25.82467	118.319	80.81049	7.330449	7.40167
FDHF	23.10006	120.4601	78.6659	7.118756	5.06522
MSR	30.61708	59.19881	51.49067	5.266035	3.213714
GHE	22.01073	116.1428	58.05779	6.760153	4.086882
HS	27.14742	127.4739	73.89467	8	6.390259
PWL	11.65842	112.4371	104.6785	6.198049	2.326264
CS	12.20694	88.2591	84.09863	6.551213	1.967786
GOC1	12.15898	88.68082	84.42666	6.514779	1.977533
GOC2	12.15898	88.68082	84.42666	6.514779	1.977533
GOC3	12.011	119.6163	114.1335	4.890023	2.303063
PA_2B	26.93677	112.6386	85.44763	7.230468	5.275181
PA_1A	26.93677	112.6386	85.44763	7.230468	5.275181
GUM	72.85171	149.4588	92.856	6.501869	10.1732
SSR	104.8461	173.5025	104.4962	2.709715	9.236858
SSAR	8.102315	47.36964	51.38798	4.524359	1.110965
TC	25.64745	125.3163	108.3916	5.924862	2.977004
MSRCR	33.68869	53.31446	49.97375	5.038495	2.968169

Table 3 Quantitative (relative) comparison of PA with popular algorithms for (a) *Swan* (b) *Notre Dame* (c) *Big Ben* (d) *Horse* images

(a)

Algos\Measures	RC	F	PQM	REMEC	RM	RSD	RE	RAG	HDI	EMEC_2
PDE_HS	1.369563	0.636212	9.215336	1.247953	1.631109	1.018691	1.159587	1.893488	6.989006	16.76189
PDE_GOC2	1.369563	0.636212	9.215336	1.247953	1.631109	1.018691	1.159587	1.893488	6.989006	16.76189
PDE_GOC3	1.225021	0.788486	9.904711	0.698589	1.442316	1.066418	1.034743	1.306275	7.320744	9.383101
PDE_PWL	1.258974	1.402977	10.00693	10.29938	1.013946	1.192704	0.986951	1.21825	5.112686	138.3362
PDE_GHE	2.345871	0.535439	8.085046	2.073571	2.46279	1.148335	1.076786	3.067447	11.31385	27.85118
PDE_CE	0.664216	0.625525	10.70477	13.08342	0.611207	0.618324	0.940466	0.941702	7.056079	175.7301
PDE_CS	1.207461	1.309071	10.09095	1.700594	1.022149	1.156748	0.994952	1.17995	3.841516	22.84154
PDE_MINMAX	0.898734	1.078303	9.667047	0.794077	0.911063	0.991162	0.958585	0.557727	4.609464	10.66566
PDE_AHE	2.465277	0.508135	7.568375	3.831895	2.369004	1.097167	1.213991	4.309845	14.60396	51.46812
PDE_CLAHE	1.67044	0.617324	8.944542	1.205058	1.525963	0.970574	1.140858	2.131676	6.402671	16.18574
CP_PDE_CLAHE	1.117264	0.760424	9.643628	1.122367	1.245954	0.973372	1.076949	1.683727	5.286975	15.07507
ADE1	1.546936	1.108687	9.578401	0.994625	1.440839	1.263899	0.939854	1.471503	2.18659	13.35931
ADE3	1.372167	1.288109	9.81832	4.734788	1.199505	1.243018	0.957465	1.335379	3.320813	63.59534
MCECR	1.302264	1.264534	9.952609	3.954112	1.162514	1.212451	0.984514	1.271859	2.993008	53.10968
MCECR_HF	1.322708	0.451882	8.866753	0.693553	2.087247	0.971179	1.110036	2.331679	5.240937	9.315461
MCECR_CLAHE	1.355817	0.660828	9.53471	0.838467	1.350698	0.944764	1.105633	1.204787	7.422742	11.26187
CLAHE	1.628192	0.593445	8.840716	1.225813	1.533186	0.953867	1.142119	2.278457	6.69303	16.46451
AHE	2.465277	0.508135	7.568375	3.831895	2.369004	1.097167	1.213991	4.309845	14.60396	51.46812
SHF	1.36406	0.492213	8.463246	0.946139	2.044878	1.003252	1.131727	2.924515	7.645274	12.70807
FDHF	1.306712	0.447208	8.913402	0.701319	2.061137	0.960081	1.115542	2.326636	5.14373	9.419773
MSR	1.648464	0.973854	8.543244		1.126875	1.047574	0.960945	2.131063	9.087314	
GHE	2.345871	0.535439	8.085046	2.073571	2.46279	1.148335	1.076786	3.067447	11.31385	27.85118
HS	2.433355	0.573	8.217422	3.256731	2.44251	1.18303	1.218645	3.060433	10.83301	43.7428
PWL	1.258974	1.402977	10.00693	10.29938	1.013946	1.192704	0.986951	1.21825	5.112686	138.3362
CS	1.277531	1.419	9.959905		1.023272	1.204999	0.970945	1.233004	5.314325	
GOC1	1.022828	1.01134	10.46848	1.006673	1.010747	1.011043	1.000652	1.012464	2.870382	13.52114
GOC2	1.022828	1.01134	10.46848	1.006673	1.010747	1.011043	1.000652	1.012464	2.870382	13.52114
GOC3	1.642267	0.700361	9.175185	0.612586	2.010868	1.186733	0.956914	1.706666	13.69751	8.227953
PA	1.026158	0.598298	9.441058	0.912874	1.472242	0.93853	1.072022	1.809898	6.314627	12.26128
GUM	1.967059	0.249363	8.3413	0.692045	3.140091	0.884885	1.169709	2.86375	7.819348	9.295204
SSR	1.500898	0.055287	8.660112	0.296004	4.499635	0.49877	0.488084	1.500135	9.328737	3.975786
SSAR	0.914774	1.422905	10.10053		0.535115	0.872593	0.598847	0.686228	12.88947	
TC	1.62517	0.740843	9.147615	0.867176	1.861492	1.17434	0.947308	1.830121	1.139818	11.64748
MSRCR	2.320929	1.404061	8.303884		0.988585	1.178148	0.769915	1.970034	10.10144	

(b)

Algos\Measures	RC	F	PQM	RM	RSD	RE	RAG	HDI
PDE_HS	0.693537	0.760818	8.700638	1.203619	0.956941	1.063044	1.096931	3.2868
PDE_GOC2	0.693537	0.760818	8.700638	1.203619	0.956941	1.063044	1.096931	3.2868
PDE_GOC3	0.858905	1.167906	8.755461	1.168492	1.168199	0.966971	1.097797	3.357777
PDE_PWL	0.950449	1.283884	8.443598	1.270297	1.277072	0.914308	1.182409	13.3033
PDE_GHE	0.637501	0.561739	8.079307	1.48324	0.912795	1.024241	1.236982	10.25374
PDE_CE	0.612668	0.609715	9.148268	0.613538	0.611623	0.902886	0.80081	4.454588
PDE_CS	0.882058	1.147753	8.70612	1.190469	1.168916	0.994289	1.137112	5.114248
PDE_MINMAX	1.001155	1.056902	8.394005	0.905408	0.978227	0.966158	0.455567	1.254058
PDE_AHE	1.054701	0.48719	5.921435	1.421224	0.83211	1.081721	3.082838	18.66341
PDE_CLAHE	0.969456	0.717363	7.87316	1.161352	0.912749	1.021272	1.589985	2.995098
CP_PDE_CLAHE	0.968509	0.864749	8.388061	1.099317	0.975004	1.031396	1.372739	1.85013
ADE1	0.872948	1.257119	8.210378	1.433421	1.342379	0.819519	1.273894	6.158379
ADE3	1.056341	1.217311	8.511933	1.284487	1.250448	0.942864	1.187752	2.694105
MCECR	1.063017	1.188	8.630466	1.234189	1.210875	0.973947	1.158825	2.023707
MCECR_HF	0.688594	0.656646	7.727534	1.56151	1.012601	1.041875	1.844814	3.751029
MCECR_CLAHE	0.979234	0.757572	9.096887	1.095982	0.9112	1.049988	0.939721	5.971683
CLAHE	0.930787	0.708789	7.818679	1.153548	0.904225	1.020482	1.659011	3.192205
AHE	1.054701	0.48719	5.921435	1.421224	0.83211	1.081721	3.082838	18.66341
SHF	0.722438	0.700565	6.972947	1.556483	1.044231	1.043552	2.399125	6.349478
FDHF	0.687472	0.651897	7.779067	1.542858	1.002888	1.043001	1.851708	3.786277
MSR	0.596804	0.670621	8.127166	0.682341	0.676456	0.758104	1.118321	15.19259
GHE	0.637501	0.561739	8.079307	1.48324	0.912795	1.024241	1.236982	10.25374
HS	0.645255	0.592017	8.316356	1.465271	0.931378	1.088459	1.235204	9.923013
PWL	0.950449	1.283884	8.443598	1.270297	1.277072	0.914308	1.182409	13.3033
CS	0.880517	1.197819	8.583178	1.249411	1.223343	0.973688	1.178194	7.157877
GOC1	1	1	9.0031	1	1	1	1	0
GOC2	1	1	9.0031	1	1	1	1	0
GOC3	0.942356	1.419723	7.99827	1.384747	1.402126	0.709756	1.235106	15.94169
PA_1A	0.701441	0.847426	7.234434	1.427373	1.099815	1.019616	2.340876	2.566798
GUM	0.950463	0.462264	6.882727	1.960716	0.952034	1.0061	1.992495	5.490489
SSR	1.317947	0.415834	5.661471	2.359099	0.990451	0.390876	1.669706	15.93422
SSAR	0.830285	0.914818	9.221785	0.548299	0.708233	0.626602	0.649376	11.76553
TC	0.780307	1.047567	8.122459	1.565128	1.28046	0.888302	1.343487	1.350291
MSRCR	0.795372	0.785739	8.104235	0.599629	0.686405	0.718852	1.1118	12.62348

(c)

Algos\Measures	RC	F	PQM	REMEC	RM	RSD	RE	RAG	HDI	EMEC_2
PDE_HS	0.829427	0.861182	9.127733	0.647361	1.246841	1.036223	1.031735	1.123506	3.585806	60.9315
PDE_GOC2	0.829427	0.861182	9.127733	0.647361	1.246841	1.036223	1.031735	1.123506	3.585806	60.9315
PDE_GOC3	1.121131	1.150689	8.981254	1.006669	1.194464	1.172372	0.998283	1.172512	2.054944	94.75051
PDE_PWL	1.38413	1.312421	8.859528		1.167811	1.238007	0.951359	1.185856	4.985989	
PDE_GHE	0.914973	0.806725	8.602648	0.138368	1.578378	1.128413	1.008794	1.306042	9.123589	13.02356
PDE_CE	0.613209	0.617855	9.920378	1.425868	0.611829	0.614835	0.911628	0.814101	1.595194	134.2068
PDE_CS	1.111493	1.141238	9.071707	1.082313	1.128948	1.135076	0.995238	1.137047	1.775194	101.8703
PDE_MINMAX	1.001677	1.022248	8.449016	0.984505	0.932356	0.976268	0.987618	0.578854	0.69743	92.6644
PDE_AHE	0.826916	0.719839	6.763662	0.245432	1.46876	1.028237	1.041779	2.648758	18.3554	23.10079
PDE_CLAHE	0.854207	0.785142	8.399892	0.175629	1.220824	0.979041	1.022436	1.599354	4.277394	16.53068
CP_PDE_CLAHE	0.978894	0.869455	8.882895	0.192719	1.104484	0.979948	1.011847	1.386206	1.421066	18.13924
ADE1	1.537905	1.207261	8.51988	1.004228	1.48824	1.340408	0.914099	1.331038	3.348789	94.52078
ADE3	1.30079	1.181521	8.766637	1.078936	1.332045	1.254528	0.972223	1.26174	3.133409	101.5525
MCECR	1.237237	1.162453	8.8801	1.0773	1.271929	1.215959	0.982371	1.215438	2.670539	101.3986
MCECR_HF	0.826165	0.584503	8.302642	0.120801	1.707307	0.998963	1.013405	1.761523	3.048799	11.37013
MCECR_CLAHE	0.84635	0.738845	9.174231	0.135545	1.162449	0.926752	1.017556	1.048444	3.175443	12.7579
CLAHE	0.876354	0.764176	8.324198	0.178226	1.186571	0.952234	1.018205	1.69593	4.169494	16.7751
AHE	0.826916	0.719839	6.763662	0.245432	1.46876	1.028237	1.041779	2.648758	18.3554	23.10079
SHF	0.837914	0.624161	7.963148	0.296767	1.69081	1.027296	1.014325	2.194935	4.642079	27.9326
FDHF	0.818236	0.581197	8.355002	0.121922	1.682435	0.988851	1.014764	1.765891	2.953714	11.47565
MSR	0.727431	0.867796	8.769987		0.855631	0.861692	0.8539	1.073397	9.426818	
GHE	0.914973	0.806725	8.602648	0.138368	1.578378	1.128413	1.008794	1.306042	9.123589	13.02356
HS	0.921329	0.830293	8.811686	0.490795	1.564476	1.139725	1.049235	1.291979	8.849393	46.19503
PWL	1.38413	1.312421	8.859528		1.167811	1.238007	0.951359	1.185856	4.985989	
CS	1.147513	1.1868	8.923026		1.166474	1.176593	0.970815	1.178214	3.612152	
GOC1	1	1	9.380909	1	1	1	1	1	0	94.12284
GOC2	1	1	9.380909	1	1	1	1	1	0	94.12284
GOC3	1.425261	1.418892	8.031775		1.444619	1.431698	0.819166	1.406477	8.152909	
PA	0.848165	0.745868	7.850542	1.012947	1.59102	1.089353	1.007621	2.362118	2.559008	95.34145
GUM	0.846792	0.380799	8.148471	0.291564	2.202314	0.915772	0.993422	1.661788	6.834022	27.44282
SSR	1.037643	0.222012	6.830193	0.94169	2.871119	0.798388	0.25043	1.117587	23.86199	88.63454
SSAR	0.794501	1.224565	9.805421		0.462071	0.752221	0.70195	0.737889	6.256646	
TC	1.179645	0.877727	8.533475	0.985197	1.769367	1.246203	0.930331	1.364808	2.06565	92.72955
MSRCR	1.105772	1.263866	8.574126		0.754414	0.976462	0.805923	1.11118	7.668157	

(d)

os\Measures	RC	F	PQM	RM	RSD	RE	RAG	HDI
PDE_HS	1.199543	0.761002	10.87293	1.287002	0.989652	1.178809	2.180977	7.99827
PDE_GOC2	1.199543	0.761002	10.87293	1.287002	0.989652	1.178809	2.180977	7.99827
PDE_GOC3	0.941169	1.233005	11.71787	1.242483	1.237735	0.981844	1.14724	1.683549
PDE_PWL	0.97175	1.391679	11.29287	1.460472	1.425661	0.95985	1.354359	13.96247
PDE_GHE	1.834633	0.414441	10.27025	1.508606	0.790714	1.046899	2.379397	16.23942
PDE_CE	0.657201	0.602841	11.95958	0.615816	0.609294	0.915546	1.38932	4.445607
PDE_CS	1.009345	1.111755	11.87911	1.114697	1.113225	1.013164	1.115969	1.076393
PDE_MINMAX	0.991636	1.016661	9.636885	0.987272	1.001859	0.954726	0.701298	1.271472
PDE_AHE	3.928653	0.322031	8.635156	1.736364	0.747772	1.20269	6.70506	24.80391
PDE_CLAHE	2.232296	0.834949	10.65871	1.098043	0.957502	1.064981	2.340915	4.978221
CP_PDE_CLAHE	1.267979	0.924334	11.43345	1.081354	0.999766	1.028619	1.83242	1.46052
ADE1	1.593979	1.454779	11.18268	1.525215	1.489581	0.878413	1.40428	5.058383
ADE3	1.223128	1.313947	11.48456	1.329909	1.321904	0.983627	1.295731	3.364533
MCECR	1.159551	1.263331	11.64886	1.268416	1.265871	1.019503	1.240194	2.013526
MCECR_HF	1.949829	0.743329	10.3957	1.586411	1.085921	1.10127	2.893722	2.998113
MCECR_CLAHE	2.114702	0.885393	10.46383	1.062191	0.969772	1.080716	1.487736	4.075951
CLAHE	1.978246	0.802087	10.57824	1.090457	0.935223	1.047569	2.483371	3.57745
AHE	3.928653	0.322031	8.635156	1.736364	0.747772	1.20269	6.70506	24.80391
SHF	2.152531	0.788162	10.06284	1.536873	1.100593	1.135217	4.309279	4.310034
FDHF	1.92543	0.733608	10.59391	1.564685	1.071385	1.102434	2.948989	3.064269
MSR	2.551987	0.639555	10.55708	0.768948	0.701274	0.815515	1.871036	18.27145
GHE	1.834633	0.414441	10.27025	1.508606	0.790714	1.046899	2.379397	16.23942
HS	2.262785	0.611701	9.796438	1.655789	1.006403	1.238906	3.720432	21.57824
PWL	0.97175	1.391679	11.29287	1.460472	1.425661	0.95985	1.354359	13.96247
CS	1.017469	1.144333	11.82769	1.146419	1.145375	1.014542	1.145652	1.568112
GOC1	1.013472	1.147793	11.81415	1.151896	1.149843	1.0089	1.151327	2.348662
GOC2	1.013472	1.147793	11.81415	1.151896	1.149843	1.0089	1.151327	2.348662
GOC3	1.001138	1.555142	10.9191	1.553725	1.554433	0.757285	1.340852	17.46785
PA_2B	2.245227	0.92565	10.65496	1.46309	1.163748	1.119734	3.071229	3.828653
PA_1A	2.245227	0.92565	10.65496	1.46309	1.163748	1.119734	3.071229	3.828653
GUM	6.072317	0.823821	8.613029	1.941356	1.264646	1.006901	5.922875	8.354441
SSR	8.739106	0.898731	7.417722	2.253666	1.423179	0.419635	5.377731	21.01206
SSAR	0.675342	0.796081	12.14461	0.615296	0.699875	0.700657	0.646808	16.43802
TC	2.13776	1.338806	10.84438	1.627764	1.476232	0.917543	1.733222	0.554686
MSRCR	2.808011	0.668918	10.54921	0.692514	0.680614	0.780278	1.728078	14.26765

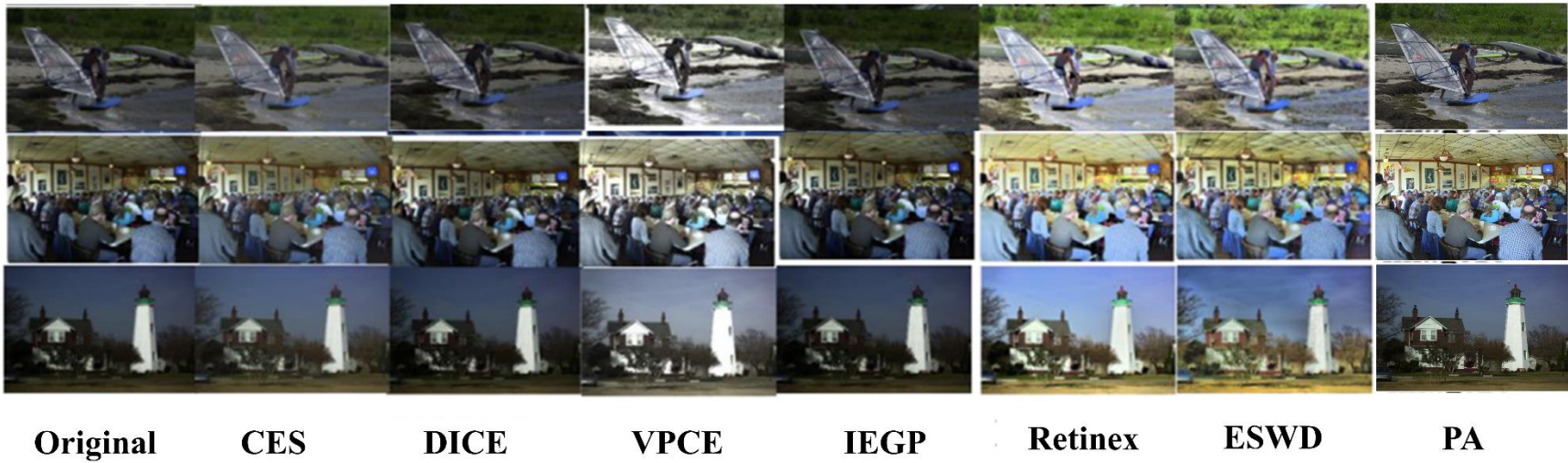


Fig. 4 (a) Swan, (b) Notre Dame (c) Big Ben (d) *Horse* images processed with various algorithms and (e) key to figures



Fig. 5 Additional results using PA

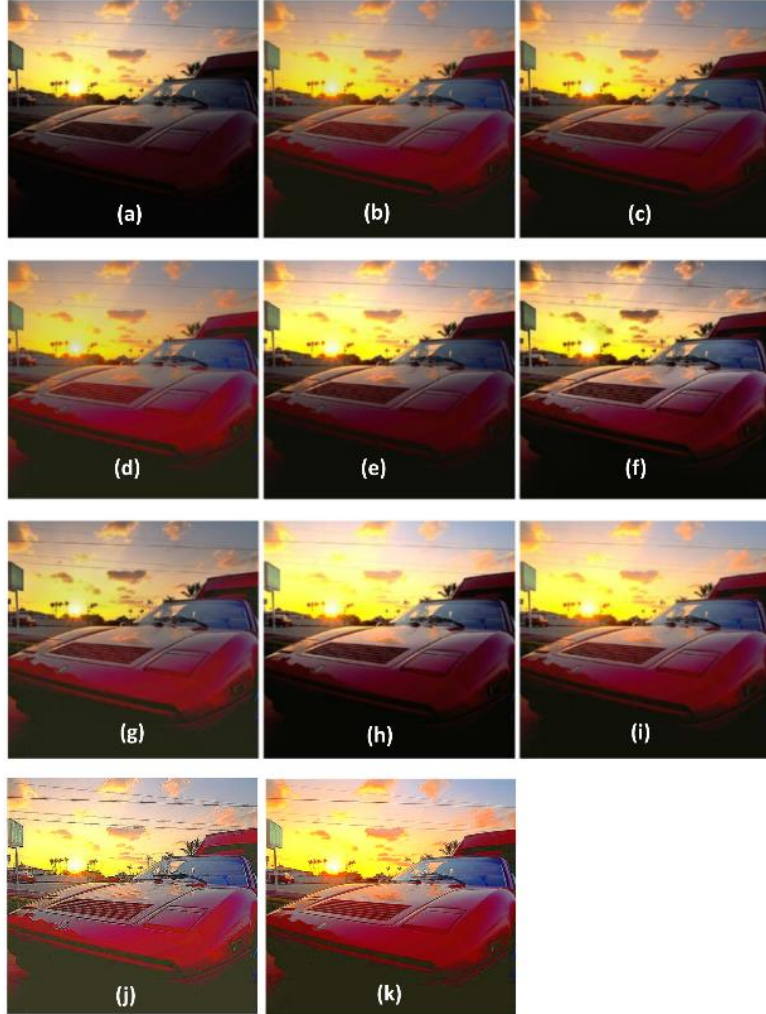


Fig. 6 Amended figure from [8] of *Ferrari* image showing (a) original image (b) to (d) SLIP using various values (e) LCS (f) CLAHE (g) LCC (h) AGC (i) PLR (j) PA

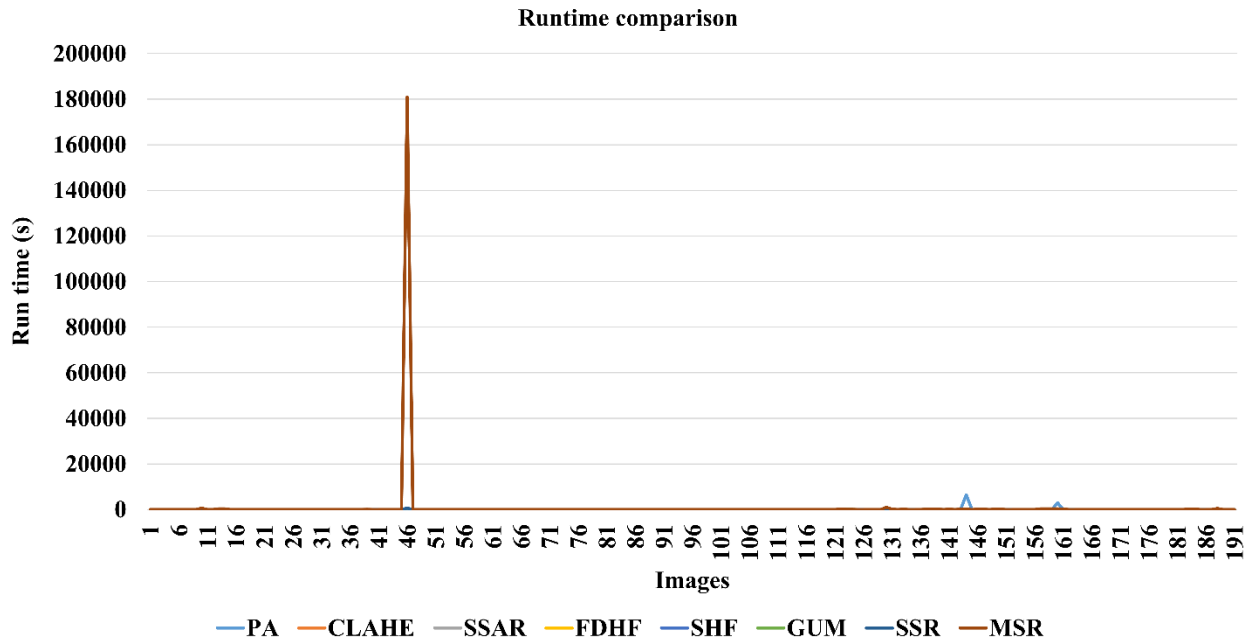
Table 4 Comparison of PA with algorithms from [8] for *Ferrari* image

	Original	SLIP $\gamma = 0.8\gamma_0$	SLIP $\gamma = \gamma_0$	SLIP $\gamma = 1.2\gamma_0$	LCS	CLAHE	LCC	AGC	PLR	PA
σ	0.2964	0.2376	0.2588	0.2113	0.3233	0.2907	0.2241	0.4099	0.3980	0.3023
μ	0.2975	0.3238	0.3126	0.3396	0.3564	0.3341	0.3595	0.4416	0.3940	0.4610
entropy	6.6430	6.5893	6.6495	6.5291	6.6551	7.1288	6.9007	6.7063	6.7826	7.0031

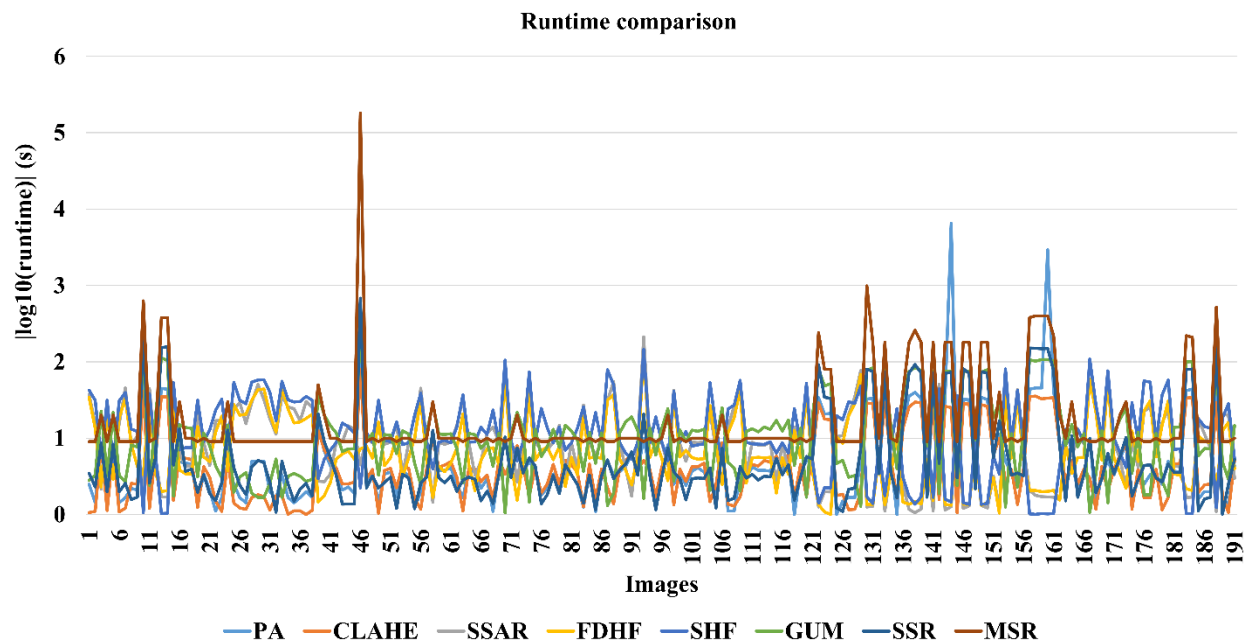
4.3 Runtime comparison

We present the plots of the various algorithms for the 195 images used to assess the time-complexity of the algorithms and their relation to the performance of PA in Fig. 7. Based on results, PA is relatively fast in most cases, where optimization goals are quickly obtained, while in some other cases, it takes longer. Moreover, the Retinex methods exhibit the longest runtimes and this increases drastically for much larger images as seen. Thus, PA outperforms several of the closed-form approaches in terms of results and time complexity if run for a single iteration or in its adaptive mode. Additionally, it can be modified to mimic the results of other algorithms. The addition of a previously developed colour enhancement function can improve its colour rendition capabilities for certain images with faded colours. its automated, adaptive, metric optimization-based approach is advantage in some cases and its disadvantage in others. Furthermore, we have presented a successful PDE-based re-interpretation of illumination correction,

dynamic range compression and contrast enhancement, easily achieved using spatial operators. Future work would involve implementing the PDE-based approach on an FPGA fabric and on a mobile embedded device platform.



(a)



(b)

Fig. 7 Runtime comparison (a) linear (b) log domain

5. Conclusion

This report has presented the results of a PDE-based log-agnostic algorithm using spatial filter operators translated as opposing PDE-based flows [51]. The algorithm is of lower complexity when compared with algorithms such as

CLAHE, GUM, SSR, and MSRCR. The proposed approach has been compared with numerous images and algorithms from the literature and show comparable performance with algorithms utilizing the logarithmic function and more complex operations. However, more work is needed to incorporate a strong local contrast enhancement operator that neither adds to the complexity nor over-enhances local regions, resulting in halos. Additionally, issues such as reduction of run-time and computational complexity of the algorithms in addition to improved image results will be the main focus in future work.

References

- [1] R. C. Gonzalez and R. E. Woods, *Digital Image Processing, 2nd edition.*: Prentice Hall, 2002.
- [2] R. C. Gonzalez, R. E. Woods, and S. L. Eddins, *Digital Image Processing Using MATLAB.*: Prentice Hall, 2004.
- [3] A. V. Oppenheim, R. W. Schafer, and T. G. Stockham, "Nonlinear Filtering of Multiplied and Convolved Signals," *Proceedings of the IEEE*, vol. 56, pp. 1264 - 1291, August 1968.
- [4] D. J. Jobson and Z-U. Rahman and G. A. Woodell, "A Multiscale Retinex for Bridging the Gap Between Color Images and the Human Observation of Scenes," *IEEE Transactions on Image Processing*, vol. 6, pp. 965 - 976, 1997.
- [5] Xueyang Fu et al., "A fusion-based enhancing method for weakly illuminated images," *Signal Processing*, vol. 129, pp. 82-96, 2016.
- [6] Se Eun Kim, Jong Ju Jeon, and Il Kyu Eomn, "Image contrast enhancement using entropy scaling in wavelet domain," *Signal Processing*, vol. 127, pp. 1-11, 2016.
- [7] Shijie Hao, Daru Pan, Yanrong Guo, Richang Hong, and Meng Wang, "Image detail enhancement with spatially guided filters," *Signal Processing*, vol. 120, pp. 789-796, 2016.
- [8] Guang Deng, "A generalized gamma correction algorithm based on the SLIP model," *EURASIP Journal on Advances in Signal Processing*, vol. 2016, no. 69, pp. 1-15, June 2016.
- [9] G. Deng, "A Generalized Unsharp Masking Algorithm," *IEEE Transactions on Image Processing*, vol. 20, no. 5, pp. 1249-1261, May 2011.
- [10] Laurent Navarro, Guang Deng, and Guy Courbebaisse, "The symmetric logarithmic Image processing model," *Digital Signal Processing*, no. 23, pp. 1337 - 1343, 2013.
- [11] Yonghun Shin, Soowoong Jeong, and Sangkeun Lee, "Efficient naturalness restoration for nonuniform illumination images," *IET Image Processing*, pp. 1-10, 2015.
- [12] Guillermo Sapiro and Vicent Caselles, "Histogram Modification via Differential Equations," *Journal of Differential Equations*, vol. 135, no. DE963237, pp. 238-268, 1997.
- [13] E. Provenzi and V. Caselles, "A wavelet perspective on variational perceptually-inspired color enhancement," *Int. J. Comput. Vis.*, vol. 106, pp. 153-171, 2014.
- [14] R. Kimmel, M. Elad, D. Shaked, K. Keshet, and I. Sobel, "A Variational framework for Retinex," *Int. J. Comput. Vis.*, vol. 52, no. 1, pp. 7-23, Apr. 2003.
- [15] M. K. Ng and W. Wang, "A total variation model for Retinex," *SIAM Journal on Imaging Science*, vol. 4, no. 1, pp. 345-365, 2011.
- [16] D. Zosso, G. Tran, and S. Osher, "A unifying Retinex model based on non-local differential operators," *Proc. of SPIE, Comput. Imag. XI*, pp. 865702-1 - 865702-16, February 2013.
- [17] D. Zosso, G. Tran, and S. J. Osher, "Non-local Retinex - A unifying framework and beyond," *SIAM J. Imag. Sci.*, vol. 8, no. 2, pp. 787-826, 2015.
- [18] Xia Len, Huanfeng Shen, Liangpei Zhang, and Qiangqiang Yuan, "A spatially adaptive retinex variational model for the uneven intensity correction of remote sensing images," *Signal Processing*, vol. 101, pp. 19-34, 2014.
- [19] Huifang Li, Liangpei Zhang, and Huanfeng Shen, "A Perceptually Inspired Variational Method for the Uneven Intensity Correction of Remote Sensing Images," *IEEE Transactions on Geoscience and Remote Sensing*, vol. 50, no. 8, pp. 3053-3065, 2012.
- [20] Jie Zhao, Yongmin Yang, and Ge Li, "The Cold Rolling Strip Surface Defect On-Line Inspection System Based on Machine Vision," in *Second Pacific-Asia Conference on Circuits, Communication and Systems (PACCS)*, Beijing, August 2010.

- [21] Rajlaxmi Chouhan, Rajib Kumar Jha, and Prabir Kumar Biswas, "Enhancement of dark and low-contrast images using dynamic stochastic resonance," *IET Image Processing*, vol. 7, no. 2, pp. 174-184, 2013.
- [22] L. Wang, L. Xiao, H. Liu, and Z. Wei, "Variational Bayesian method for Retinex," *IEEE Transactions on Image Processing*, vol. 23, no. 8, pp. 3381-3396, August 2014.
- [23] Xueyang Fu et al., "A Probabilistic Method for Image Enhancement With Simultaneous Illumination and Reflectance Estimation," *IEEE Transactions on Image Processing*, vol. 24, no. 12, pp. 4965 - 4977, December 2015.
- [24] U. A. Nnolim, "Entropy-guided Retinex anisotropic diffusion algorithm based on partial differential equations (PDE) for illumination correction," University of Nigeria, Enugu, 2017. [Online]. <http://arxiv.org/pdf/>
- [25] Rui Zhang, Xiangchu Feng, Lixia Yang, Lihong Chang, and Chen Xu, "Global sparse gradient guided variational Retinex model for image enhancement," *Signal Processing: Image Communication*, vol. 58, pp. 270-281, October 2017.
- [26] Seungyong Ko et al., "Variational framework for low-light image enhancement using optimal transmission map and combined l1- and l2-minimization," *Signal Processing: Image Communication*, vol. 58, pp. 99-110, October 2017.
- [27] Vicent Caselles, Jean-Michel Morel, Guillermo Sapiro, and Allen Tannenbaum, "Introduction to the Special Issue on Partial Differential Equations and Geometry-Driven Diffusion in Image Processing and Analysis," *IEEE Transactions on Image Processing*, vol. 7, no. 3, pp. 269-273, March 1998.
- [28] V. Patrascu and V. Buzuloiu, "Color Image Enhancement in the Framework of Logarithmic models," in *The 8th IEEE International Conference on Telecommunications (IEEE ICT2001)*, Bucharest, Romania, 2001.
- [29] C. Florea and L. Florea, "Parametric logarithmic type image processing for contrast based auto-focus in extreme lighting conditions," *Int. J. Appl. Math. Comput. Sci.*, vol. 23, no. 3, 2013.
- [30] Uche Nnolim, "FPGA Architectures for Logarithmic Colour Image Processing," Canterbury, PhD Thesis 2009.
- [31] K. Zuiderveld, "Contrast limited adaptive histogram equalization," in *Graphics Gems IV*, P. Heckbert, Ed.: Academic Press, 1994.
- [32] Mila Nikolova and Gabriele Steidl, "Fast Hue and Range preserving Histogram Specification. Theory and New Algorithms for Color Image Enhancement," *IEEE Transactions on Image Processing*, vol. 23, no. 9, pp. 4087-4100, 2014.
- [33] A. B. Baliga, "Face Illumination Normalization with Shadow Consideration," Pittsburgh, May 2004.
- [34] V. Patrascu, "Image enhancement method using piecewise linear transforms," in *European Signal Processing Conference (EUSIPCO-2004)*, Vienna, Austria, 2004.
- [35] Robert Fisher, Simon Perkins, Ashley Walker, and Erik Wolfart. (2014) HYPERMEDIA IMAGE PROCESSING REFERENCE (HIPR): Contrast Stretching. [Online]. <http://homepages.inf.ed.ac.uk/rbf/HIPR>
- [36] F.T. Arslan and A.M. Grigoryan, "Fast splitting alpha-rooting method of image enhancement: Tensor representation," *IEEE Transactions on Image Processing*, vol. 15, no. 11, pp. 3375–3384, November 2006.
- [37] Z. Chen, B. Abidi, D. Page, and M. Abidi, "Gray level grouping (GLG): an automatic method for optimized image contrast enhancement - Part II: the variations," *IEEE Transactions on Image Processing*, vol. 15, pp. 2303 - 2314, 2006.
- [38] U. Nnolim and P. Lee, "Homomorphic Filtering of colour images using a Spatial Filter Kernel in the HSI colour space," in *IEEE Instrumentation and Measurement Technology Conference Proceedings, 2008, (IMTC 2008)*, Victoria, Vancouver Island, Canada, 2008, pp. 1738-1743.
- [39] G. D. Hines, Z. Rahman, D. J. Jobson, and G. A. Woodell, "Single-scale retinex using digital signal processors," in *Global Signal Processing Conference Proceedings*, September 2004.
- [40] U. A. Nnolim, "Smoothing and enhancement algorithms for underwater images based on partial differential equations," *SPIE Journal of Electronic Imaging*, vol. 26, no. 2, pp. 1-21, March 22 2017.
- [41] Sabine Susstrunk and David Hasler, "Measuring Colourfulness in Natural Images," in *IS&T/SPIE Electronic Imaging 2003: Human Vision and Electronic Imaging VIII*, 2003, pp. vol. 5007, pp. 87-95.
- [42] U. A. Nnolim and P. Lee, "A Review and Evaluation of Image Contrast Enhancement algorithms based on statistical measures," in *IASTED Signal and Image Processing Conference Proceeding*, Kailua Kona, HI, USA, August 18-20, 2008.

- [43] Xiaole Shen, Qingquan Li, Yingjie Tan, and Linlin Shen, "An Uneven Illumination Correction Algorithm for Optical Remote Sensing Images Covered with Thin Clouds," *Remote Sensing*, vol. 7, no. 9, pp. 11848 - 11862, September 2015.
- [44] Jayanta Mukherjee and Sanjit K. Mitra, "Enhancement of Colour Images by Scaling the DCT Coefficients," *IEEE Transactions on Image Processing*, vol. 17, no. 19, pp. 1783-1794, 2008.
- [45] J. Tang, X. Liu, and Q. Sun, "A direct image contrast enhancement algorithm in the wavelet domain for screening mammograms," *IEEE J. Sel. Top. Signal Process.*, vol. 3, no. 1, pp. 74–80, 2009.
- [46] G. Anbarjafari, A. Jafari, M. N. S. Jahromi, C. Ozcinar, and H. Demirel, "Image illumination enhancement with an objective no-reference measure of illumination assessment based on Gaussian distribution mapping," *Eng. Sci. Technol. Int. J.*, vol. 18, no. 4, pp. 696–703, 2015.
- [47] N. Moroney, "Local color correction using non-linear masking," in *IS&T/SID 8th Color Imaging Conference*, Scottsdale, Arizona, 2000, pp. 108–111.
- [48] J. G. G. Salas and J. L. Lisani, "Local color correction," *Image Process. On Line*, http://www.ipol.im/pub/art/2011/gl_lcc/ 2011.
- [49] S. C. Huang, F. C. Cheng, and Y. S. Chiu, "Efficient contrast enhancement using adaptive gamma correction with weighting distribution," *IEEE Trans. Image Process.*, vol. 22, no. 3, pp. 1032–1041, 2013.
- [50] G. Deng, "Parametric generalized linear system based on the notion of the t-norm," *IEEE Trans. Image Process.*, vol. 22, no. 7, pp. 2903–2910, 2013.